J Neuroimmune Pharmacol (2017) 12:260–276
DOI 10.1007/s11481-016-9710-9

ORIGINAL ARTICLE

Complexes of Peptide Blockers with Kv1.6 Pore Domain: Molecular Modeling and Studies with KcsA-Kv1.6 Channel

O. V. Nekrasova [1,2] · A. D. Volyntseva [1] · K. S. Kudryashova [1,2] · V. N. Novoseletsky [1] · E. A. Lyapina [1] · A. V. Illarionova [2] · S. A. Yakimov [2] · Yu. V. Korolkova [2] · K. V. Shaitan [1] · M. P. Kirpichnikov [1,2] · A. V. Feofanov [1,2]

Received: 21 June 2016 / Accepted: 9 September 2016 / Published online: 17 September 2016

Abstract Potassium voltage-gated Kv1.6 channel, which is distributed primarily in neurons of central and peripheral nervous systems, is of significant physiological importance. To date, several high-affinity Kv1.6-channel blockers are known, but the lack of selective ones among them hampers the studies of tissue localization and functioning of Kv1.6 channels. Here we present an approach to advanced understanding of interactions of peptide toxin blockers with a Kv1.6 pore. It combines molecular modeling studies and an application of a new bioengineering system based on a KcsA-Kv1.6 hybrid channel for the quantitative fluorescent analysis of blocker-channel interactions. Using this system we demonstrate that peptide toxins agitoxin 2, kaliotoxin1 and OSK1 have similar high affinity to the extracellular vestibule of the K^+-conducting pore of Kv1.6, hetlaxin is a low-affinity ligand, whereas margatoxin and scyllatoxin do not bind to Kv1.6 pore. Binding of toxins to Kv1.6 pore has considerable inverse dependence on the ionic strength. Model structures of KcsA-Kv1.6 and Kv1.6 complexes with agitoxin 2, kaliotoxin 1 and OSK1 were obtained using homology modeling and molecular dynamics simulation. Interaction interfaces, which are formed by 15–19 toxin residues and 10 channel residues, are described and compared. Specific sites of Kv1.6 pore recognition are identified for targeting of peptide blockers. Analysis of interactions between agitoxin 2 derivatives with point mutations (S7K, S11G, L19S, R31G) and KcsA-Kv1.6 confirms reliability of the calculated complex structure.

Keywords Voltage-gated potassium channel · Scorpion toxins · Binding assay · Membrane protein expression · Molecular modeling · Molecular dynamics

Abbreviations

AgTx2	agitoxin-2
CLSM	confocal laser scanning microscopy
IPTG	isopropyl β-D-1-thiogalactopyranoside
KTx	kaliotoxin 1
Kv	voltage-gated potassium channel
MgTx	margatoxin
MD	molecular dynamics
OSK1	a toxin from Orthochirus scrobiculosus scorpion venom
R-AgTx2	agitoxin-2 labeled with 5(6)-carboxytetramethylrhodamine N-succinimidyl ester
RMSD	root mean-square deviation
RP	reverse-phase
TEA	tetraethylammonium chloride
TFA	trifluoroacetic acid
4AP	4-aminopyridine

Introduction

Voltage gated potassium channels (Kv) are a family of structurally similar pore forming membrane proteins which are involved in a fine control of many physiological processes

Electronic supplementary material The online version of this article (doi:10.1007/s11481-016-9710-9) contains supplementary material, which is available to authorized users.

✉ A. V. Feofanov
avfeofanov@yandex.ru

[1] Biological Faculty, Lomonosov Moscow State University, Leninskie Gory 1, Moscow 119992, Russia

[2] Shemyakin-Ovchinnikov Institute of Bioorganic Chemistry, Russian Academy of Sciences, ul. Miklukho-Maklaya 16/10, 117997 Moscow, Russia

including neuronal and muscle excitability, immune cell signaling, secretion of hormones and neurotransmitters (Hayes 2004; Park et al. 2010; Shah and Aizenman 2014). Abnormal functioning of Kv channels leads to physiological disorders and requires correction that can be often achieved with channel blockers. Consequently, Kv channels are considered as potential drug targets for the treatment of a variety of diseases such as cardiovascular, neurological, and autoimmune disorders (inherited or acquired) and cancer. For example, blocking of Kv1.1 channel provides an antitumor effect (Jang et al. 2011) and alleviates symptoms of multiple sclerosis and spinal cord injury (Hayes 2004). Kv1.3 channel blockers are considered as perspective drugs for a number of autoimmune diseases (Pérez-Verdaguer et al. 2016).

Less is known about another member of Kv1 channel family, Kv1.6, which is involved in repolarization of neuronal action potential (Glazebrook et al. 2002) in electrically-excitable cells such as neurons of the central and peripheral nervous systems (Matus-Leibovitch et al. 1996; Schmidt et al. 1999; Chung et al. 2001; Alessandri-Haber et al. 2002; Glazebrook et al. 2002), muscle cells (Davies et al. 2002) and cardiomyocytes (Brahmajothi et al. 1997). Elevated expression of Kv1.6 channels in piriform cortex interneurons largely contributes to the development of pathological neuronal conduction in the case of epilepsy (Gavrilovici et al. 2012). Inhibition of Kv1.6 that results in increased duration of the action potential (Glazebrook et al. 2002) is an attractive approach to control epileptic activity of neurons.

Peptide toxins are high affinity pore blockers of Kv channels acting at pico- and nano molar concentrations (Dutertre and Lewis 2010; Bergeron and Bingham 2012). They are widely used to probe Kv channel structure, function and tissue distribution. Potential pharmacological applications attach considerable importance to peptide pore blockers guiding a search for advanced blockers of the target channels. However, cross activity to allied Kv-channels, which is a general property of many peptide toxins, significantly complicates their applications. In this way, rational design and development of potent and highly specific pore blockers is an evident way to overcome insufficient level of their selectivity. For this, a robust method for identification of molecular determinants of toxin-channel interactions and a convenient experimental approach to study peptide-channel complexes should be integrated.

As for the method, molecular modeling can help to reveal and compare interaction interfaces of peptides with Kv1.x channels (Gordon et al. 2013; Novoseletsky et al. 2016). Currently, there is no alternative to this approach, because of the difficulties in crystallizing Kv-channels and peptide-channel complexes. Structures of KcsA, KvAP, Kv1.2, chimeric Kv1.2–2.1 channels as well as two complexes of charybdotoxin with Kv1.2–2.1 and mutated KcsA were only resolved with a high resolution (Novoseletsky et al. 2016). High structural homology of both Kv1-channels and their ligands, peptide blockers, allows one to combine a homology modeling technique with a molecular dynamics simulation to describe the features of other complexes of interest.

In turn, bioengineering systems based on KcsA-Kv1.x hybrid channels can be used to search for new blockers in animal venoms and to study blocker affinity and selectivity to a variety of related Kv1.x channels (Anh et al. 2013; Legros et al. 2000, 2002; Kudryashova et al. 2013; Hoang et al. 2014; Kuzmenkov et al. 2015). KcsA-Kv1.x (x = 1–6) channels were developed by transferring the blocker-binding site located in the S5-S6 linker region of Kv1.x into the corresponding M1-M2 linker region of the bacterial KscA channel (Legros et al. 2000, 2002). A pore-forming region (especially outer vestibule of a pore domain) in KcsA-Kv1.x channels resembles structurally and pharmacologically the corresponding region in parental Kv1.x channels. The fact that KcsA-Kv1.x (x = 1, 3) are expressed in the plasma membrane of *E.coli* in the functional tetrameric form and able to bind specifically Kv1-blockers at the surface of spheroplasts (Nekrasova et al. 2009a, 2009b) facilitated their applications. Combination of a fluorescently labeled peptide blocker and spheroplasts with membrane-embedded KcsA-Kv1.x (x = 1, 3) channels was demonstrated to produce a convenient and easy-to-use analytical system (Kudryashova et al. 2013; Kuzmenkov et al. 2015), which complemented conventional approaches to the study of channel blockers based on radioligand and patch-clamp techniques.

Here we report on the development of analogous cellular bioengineering system based on spheroplasts bearing KcsA-Kv1.6 channel and demonstrate its applicability for characterization of Kv1.6 blockers. Data on the dependence of dissociation constants of blocker-channel complexes on ionic strength are presented. Molecular modeling of the complexes of KcsA-Kv1.6 and Kv1.6 with peptide pore blockers (agitoxin 2, kaliotoxin 1, OSK1) is performed for the first time. Structural features of complexes are compared, and interaction interfaces are described. Measurements of complexations between KcsA-Kv1.6 and several single point mutants of agitoxin 2 (AgTx2) are performed to verify some of the predicted interactions in a toxin-channel complex. The obtained data can be used to rationally enhance the selectivity of constructed peptide blockers to Kv1.6 or, in opposite, to decrease involvement of this channel in interactions with peptides targeted to other Kv1 channels.

Materials and Methods

Reagents

Tetraethylammonium chloride (TEA), kaliotoxin 1 (KTx) and 4-aminopyridine (4AP) were obtained from Sigma-Aldrich

(USA). Recombinant OSK1 and AgTx2 were produced and purified as described earlier (Nekrasova et al. 2009a; Kudryashova et al. 2013). Hetlaxin isolated from the vietnamese *Heterometrus laoticus* scorpion venom (Anh et al. 2013; Hoang et al. 2014) was presented for investigation by Dr. Yu.N. Utkin. Scyllatoxin and margatoxin (MgTx) were supplied by Alomone Labs (Jerusalem, Israel). Production of recombinant single point mutants of AgTx2, namely, AgTx2(S7K), AgTx2(S11G), AgTx2(K19S), and AgTx2(R31G) is described in *Supplementary materials*. AgTx2 was labeled with 5(6)-carboxytetramethylrhodamine N-succinimidyl ester (R-AgTx2) as described earlier (Kudryashova et al. 2013).

Cloning and Expression of KcsA-Kv1.6

The gene coding for KcsA-Kv1.6, in which the 52–64 aa fragment of KcsA was changed for the 399–411 aa fragment of Kv1.6 was constructed by overlap extension PCR as described (Nekrasova et al. 2009a) using previously obtained pET28a-KcsA-Kv1.3 plasmid as a template. Kv1.6-specific primers (1.6-f and 1.6-r, Table S1), and pET-specific T7-promoter and T7-terminator universal primers were used for amplification of overlapping DNA fragments. These DNA fragments were further fused in the second round of PCR and ligated into NcoI/HindIII sites of pET28a to give pET28a-KcsA-Kv1.6 plasmid.

E.coli BL21(DE3) transformed with pET28a-KcsA-Kv1.6 were grown overnight at 30 °C in minimal M9 medium supplemented with 0.5 % glucose and 50 μg/ml of kanamycin and then inoculated in 50 ml of this medium in 0.75-l shake flasks to initial optical density of 0.05 (at 560 nm, OD_{560}). In experiments related to the optimization of KcsA-Kv1.6 membrane presentation, the cells were grown at 37 °C with aeration (250 rpm) to OD_{560} of 0.6, 0.8, 1.2, or 1.9, then induced with 15, 50 or 100 μM isopropyl-β-D-1-thiogalactoside (IPTG) and further grown for 16, 24 or 40 h at different temperatures (20, 25, 30 or 37 °C).

The level of KcsA-Kv1.6 expression was analyzed by sodium dodecyl sulfate polyacrylamide gel electrophoresis (SDS-PAGE). Densitometric analysis of SDS-PAGE gels was performed with Image J software (National Institute of Health, USA).

KcsA-Kv1.6 Binding Studies

Spheroplasts were prepared as described earlier (Kudryashova et al. 2013). Briefly, *E.coli* cells (3 ml, OD_{560} = 1.0) were treated with lysozyme (10 mg/l, 7 min) in buffer A (0.5 M sucrose, 10 mM Tris-HCl, pH 8.0), mixed with 3 ml of buffer B (0.6 mM EDTA, 10 mM Tris-HCl, pH 8.0) and incubated for 15 min at 4 °C. This procedure resulted in formation of spheroplasts ($(6 \pm 2) \times 10^8$ cells/ml) that were stabilized with 10 mM $MgCl_2$ and stored at 4 °C.

Analysis of blocker binding to KcsA-Kv1.6 was performed in a buffer containing 0.25 M sucrose, 0.1 % bovine serum albumin, 10 mM $MgCl_2$, 4 mM KCl, 0.3 mM EDTA and supplemented with either 50 mM Tris-HCl (pH 7.5), 50 mM NaCl (high salt buffer, HS-buffer) or 10 mM Tris-HCl (pH 7.5, low salt buffer, LS-buffer). KcsA-Kv1.6-spheroplasts were diluted with HS- or LS-buffer to a concentration of 1000 cells/μl.

For a saturation binding analysis, KcsA-Kv1.6-spheroplasts were incubated with increasing concentrations of R-AgTx2 in either HS- or LS-buffer. For competitive binding, spheroplasts were incubated with R-AgTx2 (1 nM in LS-buffer or 8 nM in HS-buffer) and increasing concentrations of pore blockers. Reactions mixtures were continuously stirred at room temperature during 1.5 h, transferred into wells of a flexiPERM silicon chamber (Perbio) attached to a cover slip, centrifuged for 6 min at 200×*g* and placed under a microscope.

Confocal fluorescent images of spheroplasts were recorded at ca. 0.25 μm lateral and 1.5 μm axial resolution with an inverted LSM 710 microscope (Carl Zeiss, Germany) using an αPlan-Apochromat oil immersion objective (×63, NA 1.46). Fluorescence of R-AgTx2 was excited with a He-Ne laser (543.5 nm, 12 μW on the sample) and registered in the 550–685 nm range. For quantitative analysis of R-AgTx2 binding to KcsA-Kv1.6, all parameters of the microscope that could affect recorded signal intensity were fixed. Spheroplast recognition in fluorescent images and estimation of an average fluorescence signal intensity per cell (I_f) was carried out with the ImageJ software (National Institutes of Health, USA). For each data point, I_f values of 200–250 cells were averaged to get the I_{av} value, and standard deviation was calculated. All measurements were repeated three times. Calculated dissociation constants were averaged over repeated experiments and presented as the mean ± standard error.

Computer Modeling of Channels and Complexes

Initial configurations of Kv1.6 and KcsA-Kv1.6 and their complexes with AgTx2 (KTx, OSK1) were prepared as follows. At first, models of channels and complexes were obtained by homology modeling with Modeller software (Sali and Blundell 1993) using eukaryotic channel Kv1.2 (PDB code 2A79) and the complex of charybdotoxin with eukaryotic chimeric channel Kv1.2–2.1 (PDB code 4JTA) as a templates, respectively. Next, toxins in the complex models were replaced by their experimentally obtained structures (PDB code 1AGT for AgTx2, 3ODV for KTx, 1SCO for OSK1, Fig. 1a). A voltage-sensor domain of Kv1.6 was excluded from the modeling since the analogous domain in Kv1.2 (PDB codes 2A79 and 3LUT), Kv1.2–2.1 (PDB code 2R9R) and charybdotoxin-Kv1.2–2.1 complex (PDB code 4JTA) is structurally independent from a pore domain and is not involved in toxin

binding. Homologies between pore domains of Kv1.2–2.1 and Kv1.6, Kv1.2–2.1 (Kv1.2) and KcsA-Kv1.6 are 92 % and 42 %, respectively. Homologies between charybdotoxin and AgTx2, OSK1, KTx are 45 %, 39 %, 39 %, respectively (Fig. 1b). The high homology degree meets a main requirement of homology modeling technique: protein sequence should have over 30 % identity (Xiang 2006; Webb and Sali 2016) .

Free channels and their complexes were put into the calculation cells (7 × 7 × 9 nm size) filled with approximately 11,000 water molecules (simple point charge model) and about 100 sodium and chloride ions. A minimal distance from a protein to a cell boundary was 1 nm. A potassium ion was placed in site S_2 of a channel selectivity filter. Alternative K^+ ion binding sites S_1 and S_3 were occupied by water molecules, because a presence of K^+ ions in these sites was shown to prevent positioning of a pore blocking Lys residue of toxins in the selectivity filter (Chen and Kuyucak 2009). A set of five systems was prepared for each complex differed in the angle of toxin orientation (−10, −5, 0, 5 and 10°, where a positive direction is counterclockwise) relative to the charybdotoxin orientation in the 4JTA structure. The axis of a toxin rotation was a channel pore axis. The rotation range (±10°) was chosen on a basis of preliminary calculations that revealed a low probability of larger angles of a toxin orientation in a channel binding site (data not shown).

Molecular Dynamics The Gromacs software package (www.gromacs.org) with the force field opls-AA (Jorgensen et al. 1996) was used for the molecular dynamics simulations. To optimize a system geometry, a potential energy minimization was performed by steepest descent and conjugate gradient methods followed by a system equilibration in the canonical (NPT: constant number of particles, volume, and temperature) and isothermal–isobaric (NVT: constant number of particles, pressure and temperature) ensemble. A temperature of 300 K and a pressure of 1 bar were maintained during the calculations. MD calculations were performed for 5 ns, whereas system equilibration was achieved during ca. 1 ns as followed from the analysis of the root mean-square deviation (RMSD) values of protein C_α-atoms. The residues of transmembrane helices of channels were frozen in the MD process to mimic a movement restricting action of membrane environment. We did not simulate the membrane around the channel because multiple MD studies revealed a good agreement of experimental data with simulated complexes between scorpion toxins and potassium channels obtained with such simplified approximation (Cui et al. 2002; Eriksson and Roux 2002; Wu et al. 2004; Ling and Yingliang 2007).

Data Analysis Preferred orientation of a toxin in a complex was defined by analyzing the distribution of a toxin orientation angle over the MD trajectory. Analysis of hydrophobic interactions, hydrogen and ionic bonds of a toxin having preferred orientation was performed using extended version of the Platinum software package (www.model.nmr.ru/platinum (Pyrkov et al. 2009)) for 70 selected trajectory frames. Strongly interacting residues were recognized as having considerable hydrophobic contact area (>0.2 $Å^2$) and (or) strong hydrogen bonds (score > 0.5) and (or) short-range ionic interactions (distance between ions <6 Å) after averaging of these parameters determined in the selected trajectory frames. Such residues were considered to form an interaction interface.

Results

Design of KcsA-Kv1.6 and Cellular System Based on KcsA-Kv1.6

Design of KcsA-Kv1.6 hybrid channel proposed by Legros et al. (2002) is based on the substitution of a part of the extracellular P-loop (^{52}RGAPGAQLITYPR^{64}) in a bacterial KcsA channel with the homologous ^{399}ADDDDSLFPSIPD^{411} sequence from human Kv1.6 (Fig. 1c). After this substitution homology between P-loops of KcsA-Kv1.6 and Kv1.6 achieves 83 %, and KcsA-Kv1.6 gets a capability to bind peptide pore blockers of Kv1.6 (Legros et al. 2002). P-loop contains the main determinants for the binding of outer pore blockers. Together with S5 and S6 transmembrane helices (M1 and M2 helices in KcsA) P-loop forms the pore domain of K^+-channels. Even in the transmembrane helices of a pore domain homology between Kv1.6 and KcsA achieves 23 %. Thus, KcsA-Kv1.6 could serve as a close analog of the pore domain of Kv1.6 channel. Other S1-S4 transmembrane helices of Kv1.6 constitute the voltage-sensor domain, which is structurally independent from the pore domain and does not affect the P-loop region. The voltage-sensor domain is absent in KcsA and KcsA-Kv1.6 channels.

Development of the cellular system for the study of Kv1.6 blockers was initiated assuming that KcsA-Kv1.6 expressed in *E.coli* cells incorporates into plasma membrane and forms tetramers, in which the outer pore is oriented extracellularly. Such property was previously found for KcsA-Kv1.1 and KcsA-Kv1.3 (Nekrasova et al. 2009a, 2009b) and was used to bind peptide blockers at the surface of spheroplasts. Analogously, binding of a fluorescently labeled pore blocker R-AgTx2 to *E.coli* spheroplasts, which contained KcsA-Kv1.6 in the membrane, resulted in the appearance of fluorescent cells (Fig. S1 in *Supplementary materials*). AgTx2 was selected for fluorescent labeling due to its high affinity to Kv1.6 (K_d = 36 pM (Garcia et al. 1994)). Optimal conditions of cell growth, which favoured membrane incorporation of KcsA-Kv1.6, were established as described in *Supplementary materials* (induction with 50 μM IPTG at

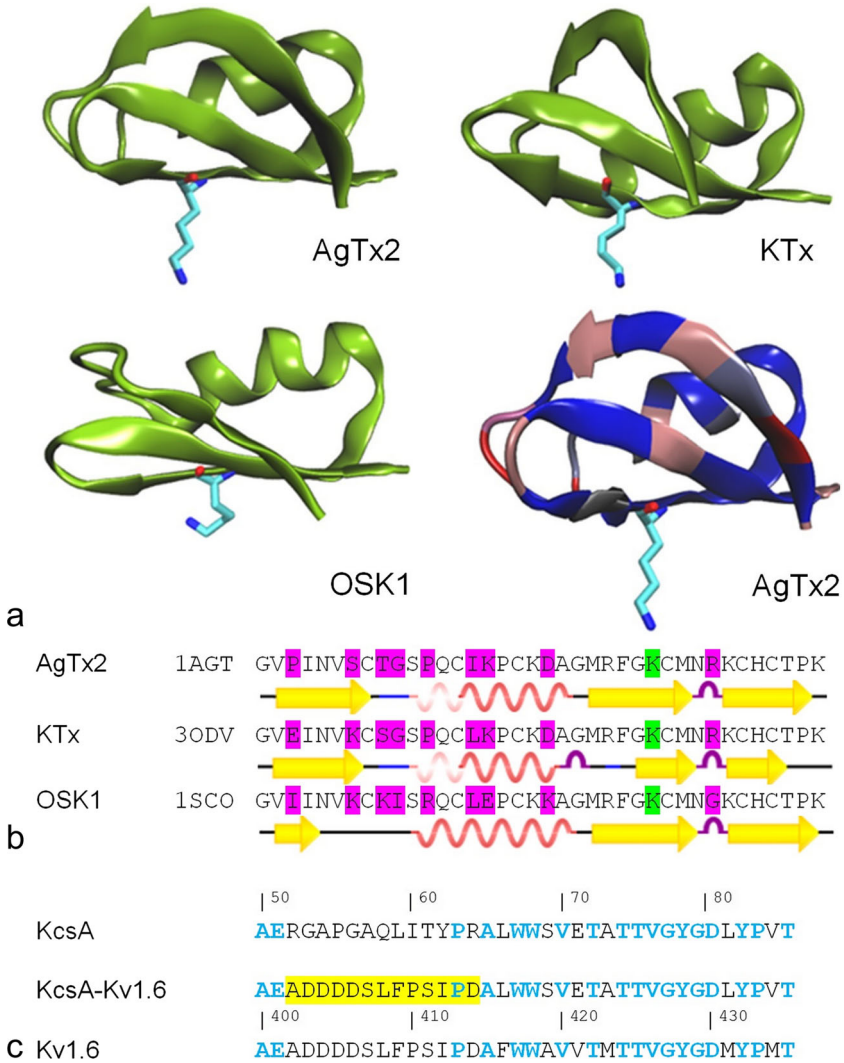

Fig. 1 Structures of AgTx2, KTx, OSK1 and P-loops of KcsA, KcsA-Kv1.6 and Kv1.6 channels. (**a**) Three-dimensional structures of the toxins in a ribbon representation with Lys27 shown by *rods*. Colored AgTx2 structure visualizes localization of variable (*red*) and conservative (*blue*) residues in the toxins. (**b**) Alignment of sequences and secondary structure elements of the toxins according to PDB files 1AGT, 3ODV and 1SCO. Differing amino acids are marked with *magenta*. Pore plugging Lys27 is marked with *green*. *Red and light red wavy lines* indicate an α-helixes and 3/10-helixes, respectively, *purple bridges* – turns, *blue lines* - bending, *yellow arrows* – β-structures, *black lines* – no assigned secondary structure. **(c)** Alignment of amino acid sequences of P-loops of KcsA, KcsA-Kv1.6 and Kv1.6 channels. *Yellow color* marks a sequence transferred from Kv1.6 to KcsA to form the KcsA-Kv1.6 channel. Residues that are identical in Kv1.6 and KcsA are marked with *blue*

OD_{560} = 0.6–0.8 and cultivation of cells at 25 °C for 24 h or longer) and were further used in our studies.

Bright staining of KcsA-Kv1.6-presenting spheroplasts with R-AgTx2 (Fig. S1d) created a basis for the reliable quantitative analysis of ligand binding. This binding can be quantified with a laser scanning confocal microscopy (LSCM). Any pore blocker of Kv1.6 will compete with R-AgTx2 for the binding to KcsA-Kv1.6 and reduce fluorescence of cells in accordance with its affinity. This competition will help to recognize pore blockers among tested compounds and characterize quantitatively their affinities to KcsA-Kv1.6 and, therefore, to Kv1.6.

Characterization of KcsA-Kv1.6 System

Staining of KcsA-Kv1.6-bearing spheroplasts with R-AgTx2 was confirmed to be related to interactions between the blocker and KcsA-Kv1.6. No binding of R-AgTx2 (50 nM) to membrane of native *E.coli* spheroplasts or to spheroplasts prepared from KcsA-expressing *E.coli* cells was observed (Fig. 2a). Following our approach approbated for KcsA-Kv1.1 and KcsA-Kv1.3 (Kudryashova et al. 2013; Kuzmenkov et al. 2015), R-AgTx2 binding to KcsA-Kv1.6 on a spheroplast membrane can be characterized with an average fluorescence intensity per cell (I_f) and parameter I_{av} being equal to I_f averaged over a measured spheroplast sampling. A dependence of I_{av} on R-AgTx2 concentration is observed in a sub- and low nanomolar range and saturated at R-AgTx2 concentration higher than 1 and 8 nM in LS- and HS-buffer, respectively (Fig. 2b). Frequency distribution of I_f at the saturation of R-AgTx2 binding is described by a normal (Gaussian) distribution (R^2 = 0.99, Fig. 2c). Therefore population of spheroplasts is uniform in terms of the amount of membrane-embedded KcsA-Kv1.6, and the I_{av} parameter is valid for evaluation of the average amount of KcsA-Kv1.6 complexes with R-AgTx2.

If KcsA-Kv1.6 receptors are titrated with R-AgTx2 ligand at the condition of [L] >> [R], where [L] and [R] are concentrations of a ligand and receptor, respectively, then the following equation can be applied for the analysis of

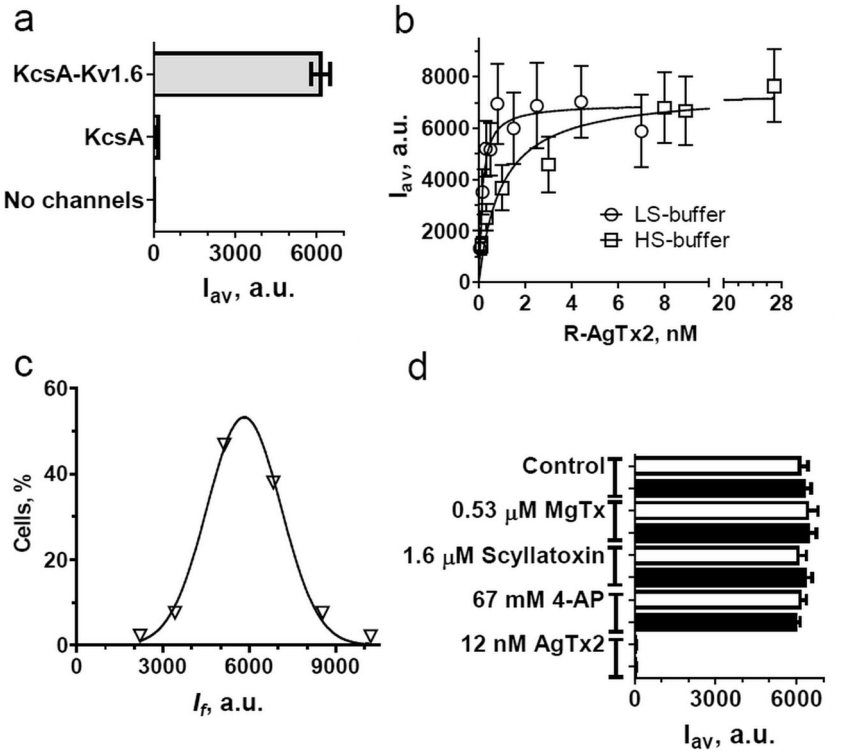

Fig. 2 Characteristics of KcsA-Kv1.6 system after optimization of membrane presentation of KcsA-Kv1.6. (**a**) Comparison of R-AgTx2 (10 nM) binding to KcsA-Kv1.6- and KcsA-bearing spheroplasts and to spheroplasts without recombinant channels in HS buffer. (**b**) Saturation curves of R-AgTx2 binding to KcsA-Kv1.6 in HS and LS buffers. (**c**) Fluorescence intensity (I_f) distribution of KcsA-Kv1.6-presenting spheroplasts stained with R-AgTx2 (10 nM) in HS buffer. Data were fitted with a normal (Gaussian) distribution ($R^2 = 0.99$). (**d**) Comparison of MgTx, scillatoxin, 4-AP and AgTx2 for their ability to displace R-AgTx2 from complexes with KcsA-Kv1.6 in HS and LS buffers (*black* and *white bars,* respectively)

ligand-receptor interactions (Kudryashova et al. 2013; Kuzmenkov et al. 2015):

$$I_{av}([L]) = I_{sat} \times [L]/(K_d + [L]) \quad (1)$$

where [L] is R-AgTx2 concentration, K_d is a dissociation constant, and I_{sat} is a fitting parameter, which is equal to the I_{av} value, when binding is saturated.

The I_{av}([L]) measurements did not depend on the concentration of cells (i.e. KcsA-Kv1.6 channels) in the 1000–10,000 cells/μl range (data not shown) and, therefore, met to the condition of [L] >> [R]. Fitting of I_{av}([L]) dependences with Eq. 1 gave us K_d of 1.0 ± 0.3 and 0.14 ± 0.04 nM in HS- and LS-buffer, respectively.

Applicability of KcsA-Kv1.6 system for recognition of pore blockers and estimation of their affinity was verified with known pore blockers of Kv1 channels, including peptides AgTx2, OSK1, KTx, MgTx and hetlaxin as well as low-molecular-weight organic molecules TEA and 4-AP. Peptide scyllatoxin, a pore blocker of a small conductance calcium activate potassium channel $K_{Ca2.3}$, was used as a negative control. AgTx2, OSK1, KTx and TEA were found to compete with R-AgTx2 for the binding to KcsA-Kv1.6 in HS- and LS-buffers (Fig. 3a, b). Hetlaxin displaced R-AgTx2 from the complexes with KcsA-Kv1.6 in LS-buffer (Fig. 3b), while 4-AP, MgTx and scyllatoxin were not active at the tested concentrations (60 mM, 0.53 μM and 1.6 μM, respectively, Fig. 2d).

The displacement of R-AgTx2 by the blockers was measured when the concentration of free R-AgTx2 was much higher than that of the bound ligand, and analyzed with the equation:

$$I_{av} = I_m / \left(1 + 10^{\left(lg[C] - lg\left(IC_{50}\right)\right)}\right) \quad (2)$$

where [C] is the concentration of the added competitive ligand, I_m is I_{av} at [C] = 0, and IC_{50} is the ligand concentration that displaces 50 % of R-AgTx2 from the complex with KcsA-Kv1.6. The estimated IC_{50} values were used to calculate the apparent dissociation constants K_{ap} of competitive ligands:

$$K_{ap} = IC_{50}/(1 + [L]/K_d) \quad (3)$$

K_{ap} value of 90 ± 20 pM obtained with KcsA-Kv1.6 for AgTx2 in HS buffer is similar to K_d of 36 pM measured for this recognized blocker in patch-clamp experiments on *Xenopus* oocytes expressing Kv1.6 channel (Garcia et al. 1994). TEA, nonspecific blocker of K^+ channels, binds to KcsA-Kv1.6 with K_{ap} being equal to 8 ± 3 mM, which corresponds well to its K_d of 1.7–7 mM determined in physiological measurements on the Kv1.6 channel (Coetzee et al. 1999). Blocker 4-AP does not compete with R-AgTx2 for the binding to KcsA-Kv1.6 (Fig. 2d) because its binding site is situated on the cytoplasmic side of a Kv1-pore domain (Kirsch et al. 1993). MgTx, which is a highly active blocker of Kv1.1-Kv1.3 channels (www.kaliumdb.org), does not bind to KcsA-Kv1.6 till submicromolar concentrations (Fig. 2d). As

expected, scyllatoxin demonstrates no binding to KcsA-Kv1.6 (Fig. 2d). To our best knowledge there are no published data concerning ability of MgTx to block Kv1.6 and scyllatoxin to interact with Kv1 channels.

According to analysis performed with KcsA-Kv1.6 channel in HS buffer, OSK1 is a high affinity blocker of Kv1.6 (K_{ap} = 190 ± 60 pM). This result is in contradiction with the published statement about inactivity of OSK1 on Kv1.6 (Mouhat et al. 2005, 2006). It has to be noted that this statement was not supported by presentation of any experimental data.

In HS buffer, affinity of KTx to KcsA-Kv1.6 (K_{ap} = 110 ± 40 pM) is similar to that of AgTx2. To our best knowledge no K_d value of KTx was determined for Kv1.6 channel in physiological experiments. At the same time Kv1.6 blocking activity of KTx was demonstrated in the measurements on mammalian cells (Hao et al. 2013).

Hetlaxin is a toxin recently found in the venom of *Heterometrus laoticus* scorpion (Hoang et al. 2014). It interacts with the extracellular vestibule of the K^+-conducting pore of KcsA-Kv1.3 and KcsA-Kv1.1 channels in HS buffer with K_{ap} values of 59 ± 6 nM and 0.8 ± 0.3 μM, respectively (Anh et al. 2013; Hoang et al. 2014). Hetlaxin has K_{ap} of

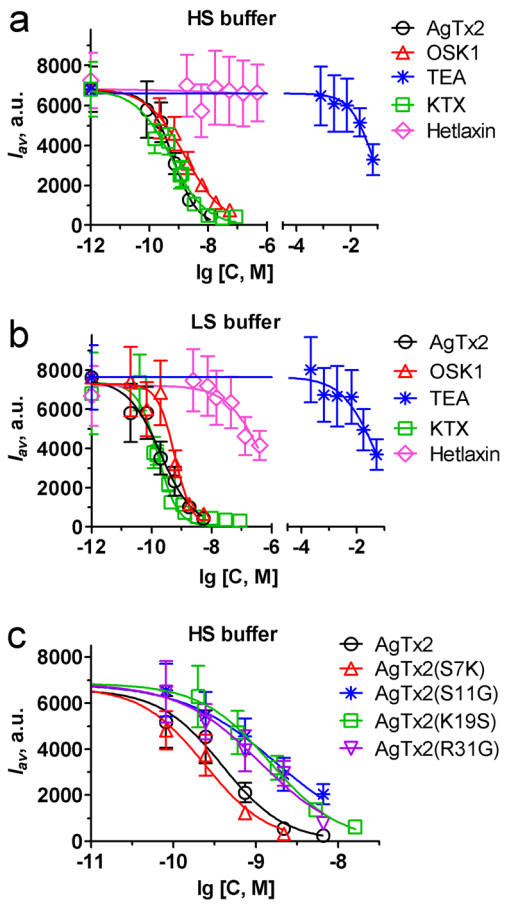

Fig. 3 Competition between R-AgTx2 and different ligands for binding to KcsA-Kv1.6-presenting spheroplasts in HS **(a, c)** and LS (**b**) buffers

60 ± 20 nM in LS buffer but does not disturb R-AgTx2 complexes with KcsA-Kv1.6 in HS-buffer even at 0.47 μM (Fig. 3a, b), thus demonstrating low affinity to Kv1.6.

Similar to hetlaxin, affinities of AgTx2, KTx and OSK1 to KcsA-Kv1.6 are several times lower in HS buffer than in LS-buffer. In LS buffer, K_{ap} values of KcsA-Kv1.6 complexes with AgTx2, KTx and OSK1 are 24 ± 14, 22 ± 12 and 70 ± 20 pM, respectively. The most evident reason of ionic strength dependence of toxin binding to KcsA-Kv1.6 is essential contribution of ionic interactions between toxin and channel charged residues into the complex formation and interference of buffer ions with these interactions. A complex with TEA is less sensitive to ionic strength. Its K_{ap} is 6 ± 2 mM in LS buffer.

The presented data show that the KcsA-Kv1.6 cellular system recognizes both small organic molecules and peptides that are able to bind to the extracellular vestibule of the Kv1.6 channel pore. This system discriminates the Kv1.6 pore blockers by their affinity and allows quantitative evaluation of blocker activity in a convenient mix-and-measure regime. The KcsA-Kv1.6 cellular system together with previously designed KcsA-Kv1.1 and KcsA-Kv1.3 systems (Kudryashova et al. 2013; Kuzmenkov et al. 2015) provide extended opportunities to search for and study of Kv1-channel blockers.

In order to extend prospective applications of the new cellular system to rational design of peptide blocker derivatives with advanced properties for functional and biomedical applications, it has to be combined (as discussed in *Introduction* section) with molecular modeling of blocker-channel complexes. Moreover, modeling of the complexes is aimed to improve our understanding of their structural determinants.

Modeling of Kv1.6 and Kcsa-Kv1.6

Kv1.6 channel belongs to the Shaker-related family of potassium channels, which have a similar structure (Tian et al. 2014). A pore domain of Kv1 channels assembled from transmembrane helices S5, S6 and the P-loop region in a homotetrameric structure is a target of peptide blockers. The pore domain of Kv1.6 is highly homologous to that of Kv1.1 (83 %), Kv1.2 (85 %) and Kv1.3 (87 %).

Since the structures of Kv1.6 and KcsA-Kv1.6 channels remain unresolved, the molecular modeling technique is intended to fill in this gap using the known structure of Kv1.2 channel (Banerjee et al. 2013) for homology modeling. We have created a model of a KcsA-Kv1.6 pore domain and repeated previously performed (Mondal et al. 2007) modeling of a Kv1.6 pore domain for direct comparison. In contrast to a previous work (Mondal et al. 2007) the structure of Kv1.6 (Kcsa-Kv1.6) pore domain obtained by homology modeling was further optimized by MD, and detailed description of structural features of Kv1.6 (Kcsa-Kv1.6), which can be important for peptide blocker binding, is presented.

Results of the modeling show that the extracellular moiety of the Kcsa-Kv1.6 (Kv1.6) pore domain is characterized by a broad and rather shallow plateau of a square shape (ca. 10 nm^2) surrounding a pore mouth. The plateau is bordered by unstructured P-loops rising up by ca. 1 nm (Fig. 4c, d). While main structural features of Kv1.6 (KcsA-Kv1.6) pore domain are similar to those of Kv1.x (x = 1–3) channels described previously (Chen and Kuyucak 2012), a net charge of Kv1.6 (KcsA-Kv1.6) exterior is much more negative (−24) as compared to the exterior of Kv1.1 (−20), Kv1.2 (−16) and Kv1.3 (−16). Here it is assumed that pKa of histidines is not significantly affected. High negative charge seems to facilitate recognition of Kv1.6 on a plasma membrane by cationic peptide blockers. Characteristic arrays of *D400*, *D401*, *D402* and *D403* (D53-D56) residues situated at the top of P-loops (Fig. 4e, f) are responsible for 16 of 24 negative charges of Kv1.6 (KcsA-Kv1.6) and can navigate a peptide blocker accelerating initial diffusion-limited stage of its binding due to multivalent ionic interactions. Here and below, to avoid repeated references to a channel type, residues of KcsA-Kv1.6 and Kv1.6 are typed by normal type and italics, respectively. Ligand and channel residues are denoted by 3-letter and 1-letter symbols, respectively.

Side chains of basic amino acids of Kv1.6 (KcsA-Kv1.6) are practically hidden (Fig. 4e, f) similar to Kv1.1 and Kv1.3 (Chen and Kuyucak 2012), whereas Kv1.2 has exposed arginine at the top of a P-loop. Distributions of aromatic residues in the exterior of Kv1.6 (KcsA-Kv1.6, Fig. 4e, f) and Kv1.x (x = 1–3) (Chen and Kuyucak 2012) channels were found to be similar except for *Y429* (Y82), which is present in Kv1.1 and Kv1.6 (KcsA-Kv1.6), but not in Kv1.3.

A presence of *L405* (L58) in a P-loop creates four well defined hydrophobic sites within the hydrophilic exterior of Kv1.6 (KcsA-Kv1.6, Fig. 4g, h), which are absent in the exterior of Kv1.x (x = 1–3) channels (Chen and Kuyucak 2012). Evidently, these hydrophobic sites can noticeably affect peptide blocker binding to Kv1.6 (KcsA-Kv1.6).

During MD simulation the channel selective filter and pore region of Kv1.6 (KcsA-Kv1.6) did not undergo significant changes, and their final structure was very similar to that of Kv1.2 in a crystal (RMSD of C_α-atoms was 1 Å). This result is in accordance with a general opinion that a pore region is highly conserved in the potassium channels of eukaryotic and prokaryotic species and has essentially the same structure (Gonzalez et al. 2012).

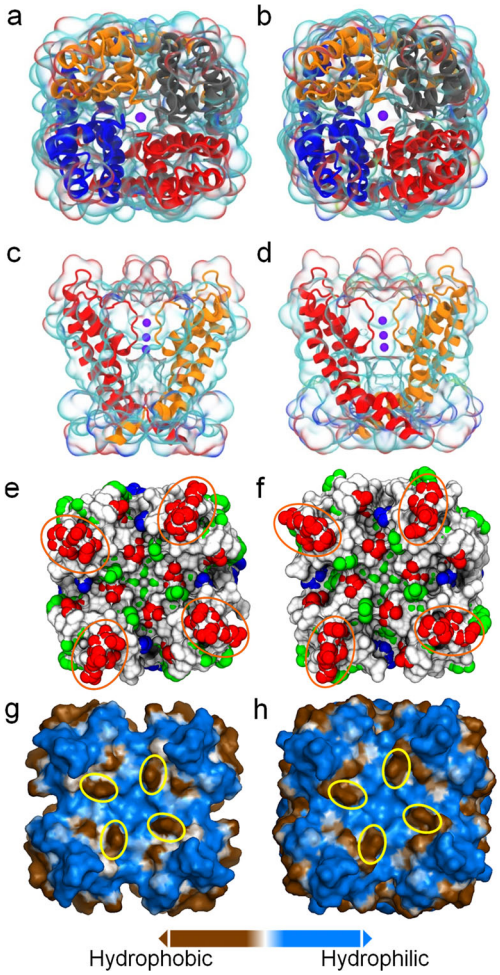

Fig. 4 Structural models of KcsA-Kv1.6 (**a**, **c**, **e**, **g**) and Kv1.6 (**b**, **d**, **f**, **h**) channels: top exterior (**a**, **b**, **e**-**h**) and side (**c**, **d**) views. *Ribbons* and *solid lines* of different color (**a**-**d**) show backbones of channels subunits. "Clouds" restrict regions of side chains. *Blue circles* (**a**-**d**) are potassium ions in a channel pore. A *side view* (**c**, **d**) is shown for clarity without a front subunit and a backbone of a back subunit. (**e**, **f**) A distribution of sidechains of exposed basic (*blue*), acidic (*red*) and aromatic (*green*) residues. A *grey color* palette encodes different layers of a channel from top (*light grey*) to deep (*dark grey*). *Orange ovals* show positions of characteristic arrays of *D400, D401, D402* and *D403* (D53-D56) residues situated at the top of P-loops. (**g**, **h**) A distribution of sidechains of exposed hydrophobic (*brown*) and hydrophilic (*blue*) residues. *Yellow ovals* indicate positions of characteristic *L405* (L58) residues in P-loops. *Color sphere* presentation is used to show sidechains

Modeling of Toxin Complexes

General Description of Complexes

According to the MD studies AgTx2, KTx and OSK1 preserved their initial secondary structure (namely, three β-strands and an α-helix crosslinked with three disulfide bridges, Fig. 1a) in complexes with KcsA-Kv1.6 and Kv1.6 (Fig. 5, 6 and 7). Rigidity of the toxin secondary structure during binding corresponds to the data reported for crystallized complexes of charybdotoxin with Kv1.2–2.1 and modified KcsA (Yu et al. 2005; Banerjee et al. 2013) as well as to molecular modeling studies of complexes of some other channels with toxins (Rashid and Kuyucak 2014).

Starting from different orientations AgTx2 and KTx relaxed in complexes with Kv1.6 (KcsA-Kv1.6) during MD experiments to the charybdotoxin orientation in the 4JTA structure, whereas OSK1 turned to −5 ° in the plane perpendicular to the

pore axis. In dynamics, RMSD of Cα-atoms of toxins in preferable orientation were ca. 0.5 Å. In the equilibrated complexes (Figs. 5, 6 and 7, S2), a flat surface formed by the second and, partially, third β-strands of the toxins was in contact with the plateau of a pore domain, whereas the toxin α-helix and first β-strand faced away from a channel pore. The second β-strand of the toxins was roughly parallel to the plateau of a pore domain (Table S3) and even produced direct hydrophobic contacts (Phe25, Met29) with some amino acids around the pore (Tables 1, 2 and 3). Lys27 of the second β-strand of the toxins preserved intrusion into the pore (Figs. 5, 6 and 7, S2) that was an essential feature of the used template (charybdotoxin complex) and had a similar intrusion depth in the studied complexes (Table S2). The toxins were bound asymmetrically relative to a channel pore: an α-helix side of the toxins touched channel P-loops rising around the plateau, whereas an opposite side (a region of the first β-strand) was far from the plateau boundary (Figs. 5, 6 and 7).

Complexes were stabilized with variegated interactions of 15–19 toxin residues with 10 channel residues (Figs. 5, 6 and 7, S2, Tables 1, 2 and 3). All channel subunits were involved in complex formation but in different extent. OSK1 formed considerable number of bonds with subunits 3 and 4, whereas for AgTx2 and KTx, interactions with subunit 3 dominated. Here number 3 was assigned to the subunit having major interactions with the α-helix of toxins, and numeration occurred clockwise if to see from an extracellular side (Figs. 5, 6 and 7).

Note that the algorithm of Kv1.6 (KcsA-Kv1.6) complex modeling was significantly modified as compared to previously published approach (Mondal et al. 2007). We performed homology modeling of channel-toxin complexes instead of molecular docking to obtain a more reliable model, optimized structures using MD and for the first time described all contacts formed between Kv1.6 (KcsA-Kv1.6) and studied toxins using advantages offered by the program Platinum.

Channel Interaction Interfaces

Channel amino acids that interact with toxins form two main clusters (Tables 1, 2 and 3, Figs. 5, 6 and 7). The first cluster is situated in the P-loop and includes three residues: *D402, D403, L405* (D55, D56, L58) in complexes with AgTx2 and OSK1; *D403, L405, P407* (D56, L58, P60) in a complex with KTx. Second cluster of interacting residues includes *Y425* and *G426* (Y78, G79) of the selective filter and four next residues (*D427, M428, Y429, M431*; D80, L81, Y82, V84) forming a plateau around the channel pore. One more residue interacting with the toxins is found in a pore helix (*D411*; D64).

It is clearly seen that patterns of interacting amino acids are similar for KcsA-Kv1.6 and Kv1.6 (Tables 1, 2 and 3, Figs. 5, 6 and 7). KcsA-Kv1.6 reproduces bundles of interactions formed by *L405*, *D427* and *Y429* in the Kv1.6 complexes with studied toxins, a particular bundle of bonds generated by *D403* in the complex with OSK1 and a rather moderate number of bonds produced with toxins by *D402*, *D411, M428* and *M431*. At the same time invariant interactions of these residues are supplemented with additional bonds that vary for KcsA-Kv1.6 and Kv1.6 (Tables 1, 2 and 3). Totally, molecular modeling predicts that 81, 77 and 75 % of bonds in (KcsA-Kv1.6)-AgTx2, (KcsA-Kv1.6)-KTx and (KcsA-Kv1.6)-OSK1 complexes are the same as in the Kv1.6-AgTx2, Kv1.6-KTx and Kv1.6-OSK1 complexes, respectively. And vice versa, 72, 93 and 73 % of bonds in the Kv1.6-AgTx2, Kv1.6-KTx and Kv1.6-OSK1 complexes are the same as in (KcsA-Kv1.6)-AgTx2, (KcsA-Kv1.6)-KTx and (KcsA-Kv1.6)-OSK1 complexes.

Among the interacting residues of Kv1.6, residues *D402, D403, L405* and *P407* of a P-loop and *Y429* can be responsible for a channel-specific modulation of peptide blocker binding, since they differ (totally or partially) from the residues situated in analogous positions of related Kv1.x (x = 1–3) channels. *D402* and *L405* are different from analogous residues in Kv1.x (x = 1–3). *P407* of Kv1.6 is present in Kv1.2 but not in Kv1.1 and Kv1.3. *D403* distinguishes Kv1.6 from Kv1.3 and partially from Kv1.1 and Kv1.2, where a homological glutamic acid residue is present. *Y429* of Kv1.6 is present in Kv1.1 but not in Kv1.2 and Kv1.3.

As mentioned above, *L405* (L58) and *Y429* (Y82) produce two remarkable bundles of interactions. *L405* (L58) forms multiple hydrophobic contacts with an every studied toxin (Tables 1, 2 and 3). From five to eight toxin residues interact with *L405* (L58). Among them there are variable toxin residues as well as Leu(Ile)15 and Arg24 that are conservative in the studied toxins. In complexes with AgTx2 and KTx, residue *L405* (L58) of subunit 3 has the highest number of hydrophobic contacts as compared to *L405* (L58) of other subunits. Residues *L405* (L58) of subunits 3 and 4 are highly involved in the OSK1 binding. A bundle of hydrophobic contacts in a P-loop is a characteristic feature of Kv1.6 (KcsA-Kv1.6) complexes.

Y429 (Y82) produces a bundle of hydrophobic contacts and hydrogen bonds with 6–8 toxin amino acids (Tables 1, 2 and 3). Residues *Y429* (Y82) of all subunits are involved in the binding of the toxins, but participation of subunit 3 prevails in the complexes with AgTx2. Conservative Leu(Ile)15, Met29 and Thr36 as well as variable residues of the toxins interact with *Y429* (Y82).

Ionic and hydrogen bonds of *D402* (D55) were found in all complexes except for the KTx-Kv1.6 complex. Multiple salt bridges and hydrogen bonds produced by *D403* (D56) are a feature of the complex with OSK1. In contrast, involvement of *D403* (D56) in the stabilization of complexes with KTx and AgTx2 is noticeably less. The single bond of *P407* (P60) was revealed in the complex with KTx only. Obviously, structural differences of peptides

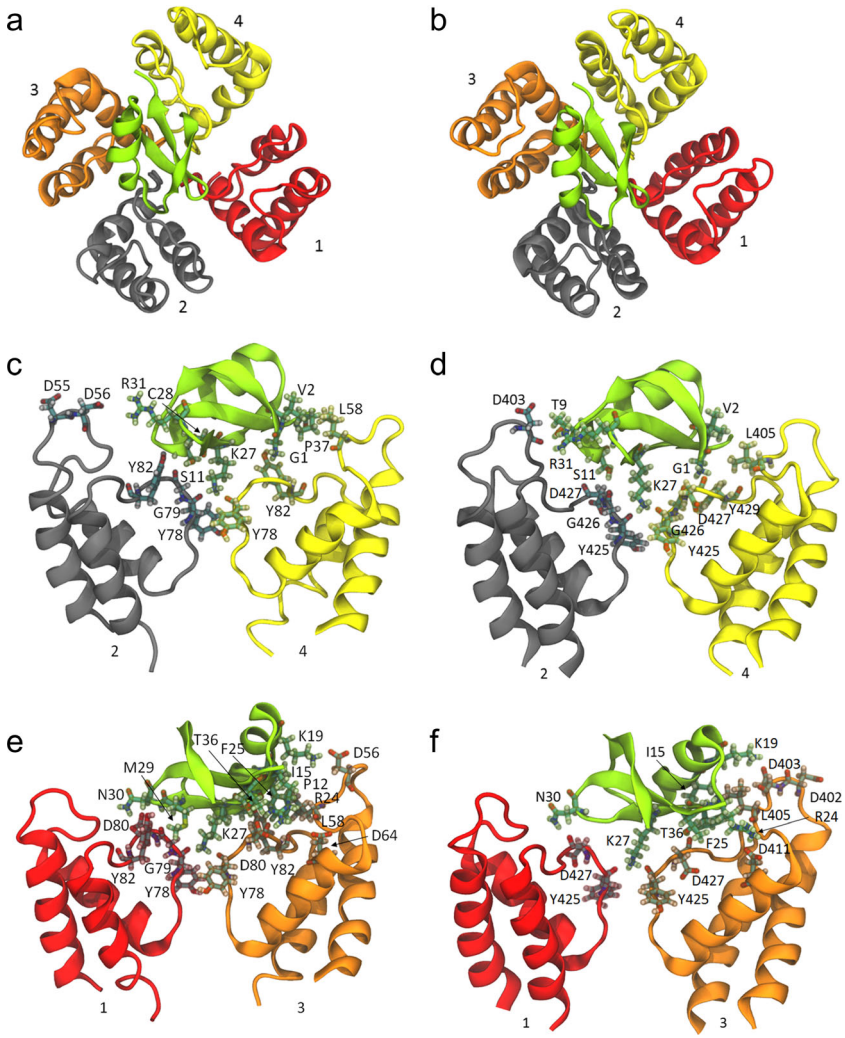

Fig. 5 Structures of complexes of AgTx2 with KcsA-Kv1.6 (**a**, **c**, **e**) and Kv1.6 (**b**, **d**, **f**): top exterior (**a**, **b**) and side (**c**-**f**) views. *Ribbons* and *solid lines* show backbones of channel subunits (*red, grey*, *orange* and *yellow*) and toxin (*green*). Front and back subunits are removed on side views (**c**-**f**) for clarity. Interacting residues are shown using stick presentation

results in multiple features of their interactions with the channel-specific residues.

Residues *D411, Y425, G426, D427* and *M428* of Kv1.6 are conservative in Kv1.x (x = 1–3) and manifest noticeable conservatism in interactions with toxins. Though there are still many gaps in understanding the structure of Kv1.x (x = 1–3) complexes with AgTx2, KTx and OSK1, the published data support this statement. Residue *D411* forms an ionic bond with invariant cationic Arg24 of AgTx2, KTx and OSK1 (Tables 1, 2 and 3) like its analog (D381) in Kv1.3-AgTx2 complex (Gao and Garcia 2003). A role of *Y425* (Tables 1, 2 and 3, Fig. 5, 6 and 7) is the same as the role of an analogous tyrosine residue in Kv1.x (x = 1–3) (Eriksson and Roux 2002; Rashid and Kuyucak 2012; Wang et al. 2015), namely, to bind a toxin Lys residue (Lys27 for AgTx2, KTx and OSK1) that occludes a channel pore. Residue *G426* is differently involved in interactions with AgTx2, KTx and OSK1 (Tables 1, 2 and 3), but its analog (G396) in Kv1.3 is also bound to Ser11 of AgTx2 (Gao and Garcia 2003). Residue *D427* produces a hydrogen bond with conservative Asn30 of the studied toxins and some additional bonds that vary for the toxins (Tables 1, 2 and 3). Similar interaction (D375-Asn30) is found in the crystal of Kv1.2-charibdotoxin complex (Banerjee et al. 2013) and predicted for KTx-Kv1.3 (D402-Asn30) (Yu et al. 2004). Hydrophobic interaction of *M428* with invariant Phe25 of the toxins (Tables 1, 2 and 3) is reproduced in the Kv1.3-AgTx2 complex (Gao and Garcia 2003).

For complexes of several toxins with channels Kv1.2–2.1 (Banerjee et al. 2013), Kv1.1 (Kohl et al. 2015), Kv1.2 (Jouirou et al. 2004) and Kv1.3 (Gao and Garcia 2003; Yu et al. 2004; Rashid and Kuyucak 2012) it was concluded that analogs of *Y425, G426* and *D427* act as an anchor on the channel surface for the bound toxins. Our data allows extension of this conclusion to Kv1.6 complexes. But in spite of the conservatism, residues *Y425, G426, D427* seem to be not sufficient for toxin binding, since KcsA channel, in which they are present in analogous positions, does not bind peptide pore blockers of Kv1-channels. R64D mutation (analogous to *D411* in Kv1.6) is required to impart toxin binding property to KcsA (MacKinnon et al. 1998). Therefore, *D411* together

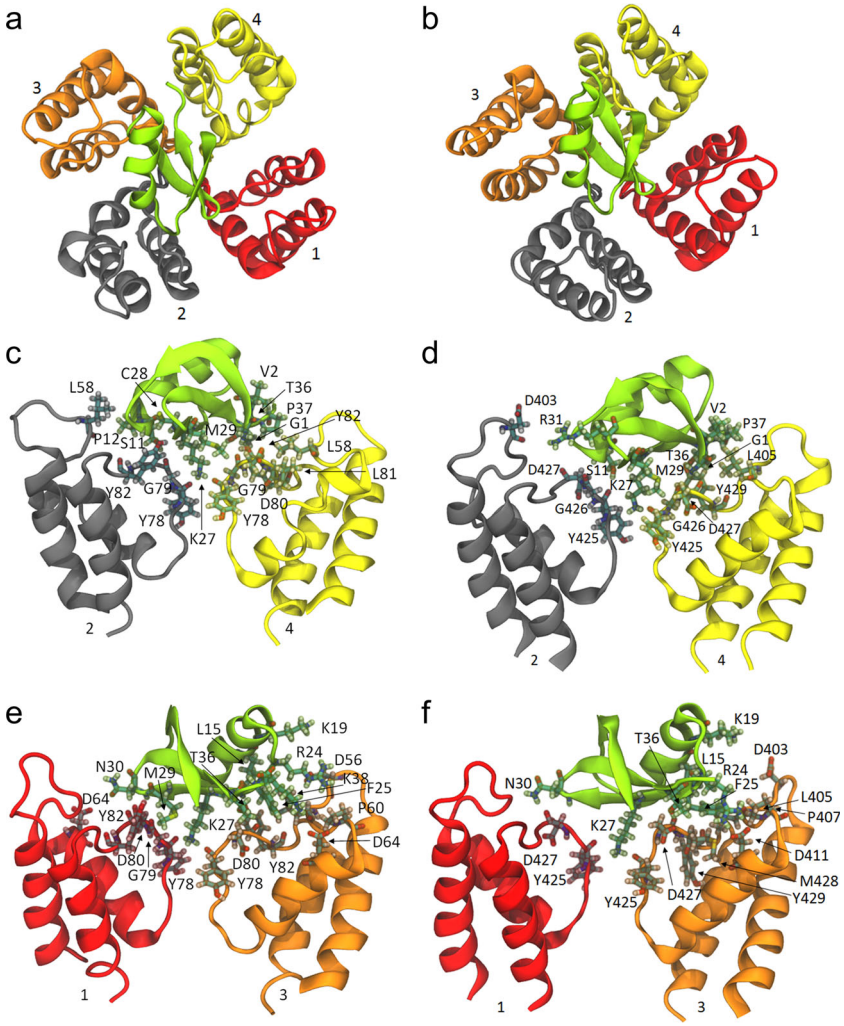

Fig. 6 Structures of complexes of KTx with KcsA-Kv1.6 (**a**, **c**, **e**) and Kv1.6 (**b**, **d**, **f**): top exterior (**a**, **b**) and side (**c**-**f**) views. *Ribbons* and *solid lines* show backbones of channel subunits (*red*, *grey, orange* and *yellow*) and toxin (*green*). Front and back subunits are removed on side views (**c**-**f**) for clarity. Interacting residues are shown using stick presentation

with *Y425, G426* and *D427* should be considered as a basic docking assembly for toxins in Kv1.x (x = 1–3) and Kv1.6. In Kv1.6, in addition to bonds of *Y425* and *D411* described above, hydrogen and, surprisingly, hydrophobic interactions are realized between *D427* and five (OSK1) or six (KTx, AgTx2) toxin residues. Next, *G426* produces either hydrophobic contacts (OSK1) or both hydrophobic contacts and hydrogen bonds (AgTx2, KTx) with three toxin residues.

During optimization of complexes in MD experiments, the structure of a selective filter of KcsA-Kv1.6 (Kv1.6) channel did not undergo significant changes (RMSD of Cα atoms =1 Å), whereas the structure of P-loops varied greater (RMSD of Cα atoms =2.5 Å). Similar to Kv1.x (x = 1–3) channels, selective filter of Kv1.6 (KcsA-Kv1.6) is a very conservative and rigid region that is not adjusted to toxins, and formation of complexes within this region corresponds well to a "lock and key" mechanism. P-loops are much more tunable to different interactions with toxin residues. In the studied complexes, P-loop of subunit 1 has a greatest mobility that can be explained by the least number of bonds formed between subunit 1 and toxins (Tables 1, 2 and 3).

Features of Toxin Interactions with Kv1.6 and KcsA-Kv1.6

Interactions of Homologous Residues of Toxins

Representatives of αKTx3 subfamily of scorpion toxins, AgTx2, OSK1 and KTx, are highly homologous: 29 of 38 residues are invariant in all three peptides, 34 residues are invariant in AgTx2 and KTx (Fig. 1). At the same time, twelve invariant residues do not participate directly in the binding of the toxins to Kv1.6 (KcsA-Kv1.6). Their primary role (together with other homologous residues) seems to be maintaining a characteristic secondary structure as well as its proper spatial organization that are essential factors contributing to toxin binding to both Kv1.6 (KcsA-Kv1.6) and Kv1.x (x = 1–3). Among interacting amino acids seven homologous toxin residues (Leu (Ile)15, Arg24, Phe25, Lys27, Met29, Asn30, Pro37) form a network of bonds, which is reproduced in all studied complexes and includes one ionic, multiple hydrophobic and several hydrogen bonds (Tables 1, 2 and 3). This steady interaction network is complemented with additional bonds of the invariant

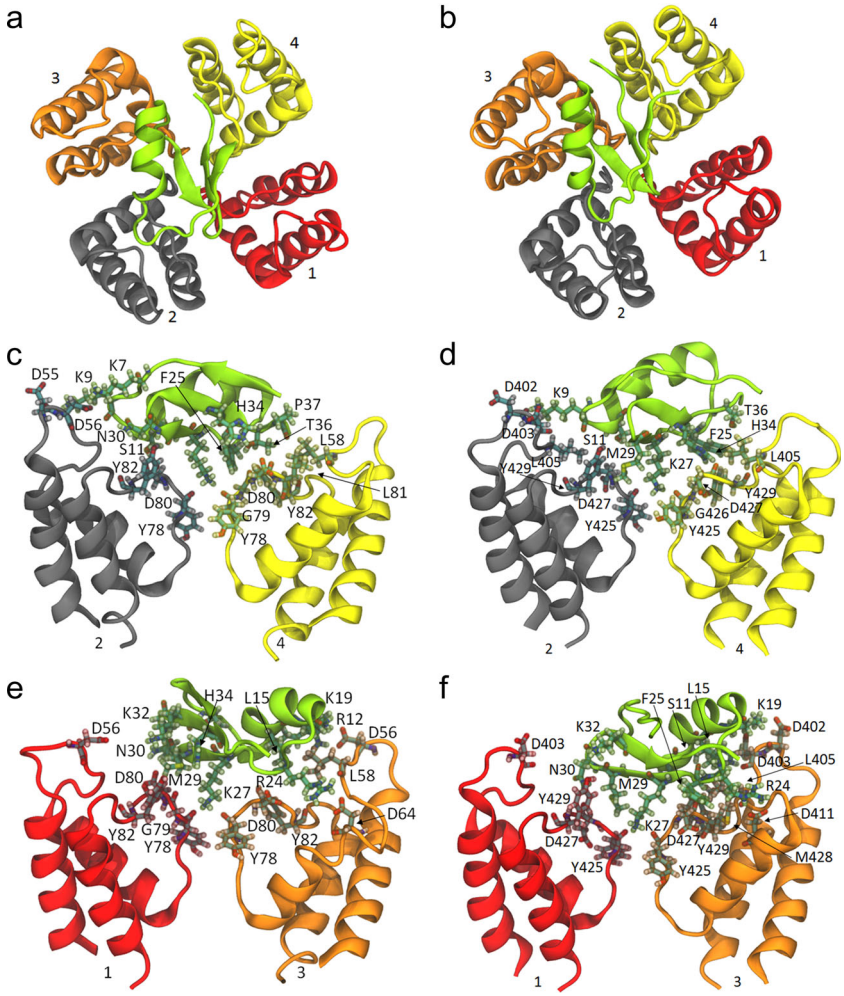

Fig. 7 Structures of complexes of OSK1 with KcsA-Kv1.6 (**a**, **c**, **e**) and Kv1.6 (**b**, **d**, **f**): top exterior (**a**, **b**) and side (**c**-**f**) views. *Ribbons* and *solid lines* show backbones of channel subunits (*red*, *grey*, *orange* and *yellow*) and toxin (*green*). Front and back subunits are removed on side views (**c**-**f**) for clarity. Interacting residues are shown using stick presentation

residues, which vary from toxin to toxin. In particular, Phe25 and Met 29 are involved in several additional interactions that differ for AgTx2, KTx and OSK1 (Tables 1, 2 and 3).

Five residues (Leu (Ile)15, Arg24, Phe25, Lys27 and Met 29) are especially prominent in the network because they produce knots of interactions (three and more bonds) in all studied complexes (Tables 1, 2 and 3). His34 in OSK1 and Thr36 in KTx produce toxin-specific knots of interactions.

If we compare AgTx2 and KTx complexes only, Gly1, Val2, Ser11 and Thr36 are added to the list of invariant residues that produce similar bonds. This extended similarity of interactions is explained by highest homology and the same orientation of AgTx2 and KTx in the binding site of Kv1.6 (KcsA-Kv1.6).

Most of residues forming the steady interaction network are situated in the second β-sheet having 100 % homology in the studied toxins (Fig.1b) and producing extensive and tight contact with a plateau around the channel pore (Tables 1, 2 and 3, S2). It is reasonable to suppose that the steady interaction network formed by invariant residues is a basis of complexes of AgTx2, OSK1 and KTx with Kv1.6 (KcsA-Kv1.6) and probably with other Kv1-channels. In accordance with this supposition, involvement of Leu15, Arg24, Phe25, Lys27, Met29 and Asn30 in KTx binding to Kv1.3 was determined experimentally (Aiyar et al. 1995; Hidalgo and Mackinnon 1995; Naranjo and Miller 1996; Ranganathan et al. 1996) and demonstrated with molecular docking (Aiyar et al. 1996). Molecular modeling predicts that Arg24, Phe25, Lys27, Met29 and Asn30 of AgTx2 interact with Kv1.3 (Lipkind and Fozzard 1997; Gao and Garcia 2003). Mutations of Arg24, Phe25, Lys27, Asn30 and Pro37 were shown to decrease considerably the AgTx2 binding to a Shaker K^+ channel from Drosophila (Gross and Mackinnon 1996; Ranganathan et al. 1996). Theoretical functional maps of OSK1 complexes with Kv1.x (x = 1–3) channels highlight importance of the following interactions: Arg24, Lys27 and Met29 with Kv1.1; Arg24, Phe25, Lys27 and Met29 with Kv1.2; Arg24, Phe25, Lys27, Met29 and Asn30 with Kv1.3 (Mouhat et al. 2005).

Interactions of Toxin Variable Residues

Variable amino acids in the studied toxins are: residues 3, 7, 9 and, partially, 15 for KTx versus AgTx2; residues 3, 7, 9, 10, 16, 20 and 31 for OSK1 versus AgTx2 and KTx (Fig. 1).

Table 1 AgTx2 interactions with KcsA-Kv1.6 and Kv1.6 according to molecular modeling

AgTx2 residues	KcsA-Kv1.6 residues	Kv1.6 residues
Gly1		Gly426(3):HB
	Asp80(4): HB*	Asp427(3):HB*
	Tyr82(3):HB*	Tyr429(3):HB*
Val2	Leu58(3):HPC*	Leu405(3):HPC*
Thr9		Asp427(3):HB
	Tyr78(2):HB	
Ser11	Gly79(2):HB*	Gly426(2):HB*
	Asp80(2):HB	
	Tyr82(3):HB*	Tyr429(3):HB*
Pro12	Tyr82(3):HPC	w.i.
	Val84(3):HPC	
Ile15	**Leu58(3):HPC***	**Leu405(3):HPC***
	Tyr82(3):HPC*	**Tyr429(3):HPC***
	Val84(3):HPC*	**Met431(3):HPC***
Lys19	Asp55(3):HB, ION*	Asp402(3):ION*
		Leu405(3):HPC
Arg24	**Leu58(3):HPC***	**Leu405(3):HPC***
	Asp64(3):HB, ION*	**Asp411(3):HB, ION***
		Met428(3):HPC
Phe25	Leu58(3):HPC*	Leu405(3):HPC*
	Asp80(3):HPC*	**Asp427(3):HPC***
	Leu81(3):HPC*	**Met428(3):HPC***
	Tyr82(3,4):HPC*	**Tyr429(3):HPC***
		Met431(3):HPC
Gly26	Tyr82(3):HB	n.i.
Lys27	**Tyr78(1, 2, 3, 4):HB***	**Tyr425(1, 2, 3, 4):HB***
Cys28	**Tyr82(2):HB***	**Tyr429(2):HB***
Met29	Gly79(4):HPC*	Gly426(4):HPC*
	Asp80(4):HPC*	Asp427(3):HPC*
	Tyr82(1):HPC*	**Tyr429(1):HPC, HB***
Asn30	Gly79(1):HB	
	Asp80(1):HB*	**Asp427(4):HB***
		Tyr429(4):HB
Arg31	Asp55(2):ION	
	Asp56(2):HB, ION*	Asp403(2):ION*
	Asp64(1):ION*	Asp411(1):ION*
Thr36	Asp80(3):HB*	Asp427(3):HB*
	Tyr78(4):HB	
		Tyr429(3):HPC
Pro37	**Leu58(4):HPC***	**Leu405(3):HPC***
		Tyr429(3):HPC
	Val84(3):HPC*	Met431(1):HPC*
Lys38	Asp64(3):ION	

HB hydrogen bond, *HPC* hydrophobic contact, *ION* ionic bond, *w.i.* weak interactions, *n.i.* no interactions. A channel subunit number is shown in parentheses. Asterisks mark interactions that are reproduced for both channels. Interactions, which are identical in all complexes of the studied toxins with Kv1.6 and KcsA-Kv1.6, are shown in bold

As mentioned above Pro3/Asp3 and Ser7/Lys7 of AgTx2/KTx do not interact with Kv1.6 (KcsA-Kv1.6) (Tables 1 and 2). Interactions of Ile15/Leu15 of AgTx2/KTx with Kv1.6 (KcsA-Kv1.6) are practically identical (Tables 1 and 2). Thr9 of AgTx2 forms a hydrogen bond with a channel, whereas Ser9 of KTx does not participate in the binding. Therefore, variable amino acids in AgTx2 and KTx do not introduce noticeable differences in the interactions of these toxins with Kv1.6 (KcsA-Kv1.6). This is a definite reason of similar affinities of AgTx2 and KTx to Kv1.6 pore revealed with the KcsA-Kv1.6 channel. Like 3D structure (Fig. 1a), which is preserved in complexes (Figs. 5 and 6), and similar repertoire of bonds formed by homologous residues (Tables 1 and 2) are two other essential factors that equalize interactions of AgTx2 and KTx with Kv1.6 pore.

As for OSK1 (Table 3), variable residues 16, 20 and 31 were not involved in the interactions with Kv1.6 (KcsA-Kv1.6). Variable residues 3, 7, 9 and 10 contributed to the interactions producing hydrophobic contacts (Ile3 and Ile10) or forming hydrogen and ionic bonds (Lys7 and Lys9) with channel residues. This should enhance OSK1 binding to the channel as compared to AgTx2 with non-interacting residues 3,7 and 10, but there are additional essential differences in the bonds produced by these toxins that result finally in slightly weaker affinity of OSK1 to Kv1.6 pore. In particular, Val2, Gly26 and Arg31 participate in the interactions of AgTx2, whereas Cys8, Lys32 and His34 are involved in the binding of OSK1.

Interactions of Toxins with L405 (L58) of a Channel

As pointed out above hydrophobic sites in the P-loops formed by *L405* (L58) are characteristic feature of Kv1.6 (KcsA-Kv1.6). This feature is recognized by toxins. Five-six amino acids of toxins minimize unfavorable exposure of hydrophobic groups by forming hydrophobic contacts with *L405* (L58) of a channel (Tables 1, 2 and 3). The contacts of Ile15(Leu15), Arg24 and Pro37 are reproduced for all toxins. AgTx2 and KTx have additional similar hydrophobic interactions of Val2 and Phe25 with *L405* (L58). Hydrophobic interactions of OSK1 with *L405* (L58) are strengthened by Thr36 as well as by Cys8 and Lys19 or Lys9 and Ile10 in the case of KcsA-Kv1.6 or Kv1.6, respectively.

Interactions of Toxin Charged Residues

Positively charged amino acids of toxins are supposed to play an essential role in channel recognition, navigation and binding. AgTx2, OSK1 and KTx have a high positive charge, but differ in amount and distribution of charged residues (Fig. 1b). As compared to least charged AgTx2, OSK1 has two additional cationic amino acids, whereas KTx has one cationic and one anionic additional residues. No direct relationships were

Table 2 KTx interactions with KcsA-Kv1.6 and Kv1.6 according to molecular modeling

KTx residues	KcsA-Kv1.6 residues	Kv1.6 residues[§]
Gly1	Gly79(4):HB*	Gly426(4):HB*
	Asp80(4):HB, ION*	Asp427(4):HB*
	Tyr82(3):HB*	Tyr429(3):HB*
Val2	Leu58(4):HPC*	Leu405(3):HPC*
Ser11		Tyr425(2):HB
	Gly79(2):HB*	Gly426(2):HB*
	Asp80(2):HB*	Asp427(2):HB*
Pro12	Leu58(3):HPC	
		Met428(3):HPC
Leu15	**Leu58(3):HPC***	**Leu405(3):HPC***
	Tyr82(3):HPC*	**Tyr429(3):HPC***
	Val84(3):HPC*	**Met431(3):HPC***
Lys19	Asp55(3):HB, ION	
	Asp56(3):ION*	Asp403(3):ION*
Arg24	Asp56(3):ION*	Asp403(3):HB, ION*
	Leu58(3):HPC*	**Leu405(3):HPC***
	Asp64(3):ION*	Asp411(3):ION*
Phe25	Leu58(3):HPC*	Leu405(3):HPC*
	Pro60(3):HPC*	Pro407(3):HPC*
	Asp80(3):HPC*	**Asp427(3):HPC***
	Leu81(3):HPC*	**Met428(3):HPC***
	Tyr82(3):HPC*	**Tyr429(3):HPC***
Gly26	Tyr82(3):HPC, HB*	Tyr429(3):HPC, HB*
Lys27	**Tyr78(1, 2, 3, 4):HB***	**Tyr425(1, 2, 3, 4):HB***
Cys28	Tyr82(2):HB	n.i.
Met29	Gly79(4):HPC*	Gly426(4):HPC*
	Asp80(4):HPC*	Asp427(4):HPC*
	Tyr82(1):HPC*	**Tyr429(1):HPC***
Asn30	Gly79(1):HPC	
	Asp80(1):HB*	**Asp427(1): HB***
Arg31	Asp56(2):HB, ION*	Asp403(2):HB, ION*
	Asp64(1):ION	
	Asp80(1):ION*	Asp427(1):ION*
Thr36	Asp80(3):HPC, HB*	Asp427(3):HPC, HB*
	Tyr82(4):HPC, HB*	Tyr429(4):HPC, HB*
	Val84(3):HPC	
Pro37	**Leu58(3):HPC***	**Leu405(3):HPC***
	Tyr82(4):HPC	
	Val84(3):HPC*	Met431(3):HPC*
Lys38	Asp64(3):ION	n.i.

HB hydrogen bond, *HPC* hydrophobic contact, *ION* ionic bond, *n.i.* no interactions. A channel subunit number is shown in parentheses. Asterisks mark interactions that are reproduced for both channels. Interactions, which are identical in all complexes of the studied toxins with Kv1.6 and KcsA-Kv1.6, are shown in bold

observed between a number of cationic and anionic amino acids and toxin affinities. Some of charged amino acids

Table 3 OSK1 interactions with KcsA-Kv1.6 and Kv1.6 according to molecular modeling

OSK1 residues	KcsA-Kv1.6 residues	Kv1.6 residues
Gly1		Asp403(4):ION
	Asp80(4):ION	
Ile3	w.i.	Leu405(4):HPC
Lys7	Asp56(2):HB, ION*	Asp403(2):ION*
Cys8	Leu58(1):HPC	n.i.
Lys9	Asp55(2):HB, ION*	Asp402(2):HB, ION*
		Asp403(2):ION
		Leu405(4):HPC
Ile10	w.i.	Leu405(2):HPC
Ser11	Asp80(2):HB*	Asp427(2):HB*
		Tyr429(2):HB
Arg12	Asp56(3):HB, ION*	Asp403(3):HB, ION*
Leu15		Asp403(3):HPC
	Leu58(3):HPC*	**Leu405(3):HPC***
	Tyr82(3):HPC*	**Tyr429(3):HPC***
	Val84(3):HPC*	**Met431(3):HPC***
Lys19		Asp402(3):HB, ION
	Asp56(3):HB, ION*	Asp403(3):HB, ION*
	Leu58(3):HPC	
Arg24	**Leu58(4):HPC***	**Leu405(4):HPC***
	Asp64(4):HB, ION*	**Asp411(4):HB, ION***
	Asp80(4):HB, ION	
Phe25	Gly79(3):HPC	Gly426(3,4):HPC*
	Asp80(3):HPC*	**Asp427(3):HPC***
	Leu81(3):HPC*	**Met428(3,4):HPC***
	Tyr82(4):HPC*	**Tyr429(3,4):HPC***
Lys27	**Tyr78(1,2,3,4):HB***	**Tyr425(1,2,3,4):HB***
Cys28	Tyr82(2):HB, HPC	n.i.
Met29	Gly79(1):HPC	Gly426(4):HPC
	Asp80(4):HPC*	Asp427(4):HPC*
	Tyr82(1):HPC*	**Tyr429(1,4):HPC***
Asn30	**Asp80(1):HB***	**Asp427(1):HB***
	Tyr82(1):HB*	Tyr429(1):HB*
Lys32	Asp56(1):ION*	Asp403(1):ION*
	Tyr82(1):HPC, HB*	Tyr429(1):HB*
His34		Leu405(4):HPC
	Gly79(4):HB	Gly426(4):HPC*
	Asp80(4):HB*	Asp427(4):HPC, HB*
	Tyr82(4):HPC*	Tyr429(4):HPC*
Thr36	Leu58(3):HPC*	Leu405(4):HPC*
	Tyr82(4):HPC*	Tyr429(4):HPC*
		Met431(4):HPC
Pro37	**Leu58(4):HPC***	**Leu405(4):HPC***
Lys38	Val84(4):HPC	n.i.

HB hydrogen bond, *HPC* hydrophobic contact, *ION* ionic bond, *w.i.* weak interactions, *n.i.* no interactions. A channel subunit number is shown in parentheses. Asterisks mark interactions that are reproduced for both channels. Interactions, which are identical in all complexes of the studied toxins with Kv1.6 and KcsA-Kv1.6, are shown in bold

(including variable) do not produce bonds with Kv1.6 (KcsA-Kv1.6): Lys32 and Lys38 in AgTx2; Glu3, Lys7 and Lys32 in KTx; Glu16 and Lys20 in OSK1 (Tables 1, 2 and 3). Among invariant cationic residues Lys19 and, especially, Arg24 and Lys27 are involved (see above) in the binding in all complexes (Tables 1, 2 and 3). Interactions of other charged amino acids vary for the studied toxins and sometimes differ for Kv1.6 and KcsA-Kv1.6 (Tables 1, 2 and 3). Ionic bonds of Arg31 contribute to particular interactions of AgTx2 and KTx with Kv1.6 and KcsA-Kv1.6 as compared to OSK1, which lacks this residue. Arg24 of KTx produces a specific salt bridge in addition to invariant one (Table 2). Lys7, Lys9, Arg12 and Lys32 of OSK1 form a set of distinctive ionic bonds with aspartates of the D-array of Kv1.6 (KcsA-Kv1.6).

As discussed above, a D-array is a characteristic feature of Kv1.6 (KcsA-Kv1.6), and cationic amino acids of the studied toxins recognize it producing ionic and hydrogen bonds with *D402*(D55) and *D403*(D56). This recognition is most pronounced for OSK1 (Table 3), in which five cationic residues form the extended set of interactions with *D402*(D55) and *D403*(D56). Two and three cationic residues interact with these aspartates in AgTx2 and KTx, respectively (Tables 1, 2).

Seven (eight) of ten charged residues of OSK1 participate in complexation with Kv1.6 (KcsA-Kv1.6), and a number of ionic bonds is highest in these complexes as compared to the complexes with AgTx2 and KTx. AgTx2 forms the least number of ionic bonds in the complexes, but its affinity is slightly higher than that of OSK1. For certain, affinities of the toxins to Kv1.6 (KcsA-Kv1.6) are defined not only by ionic interactions, but also by the combination of hydrogen bonding and hydrophobic interactions (Tables 1, 2 and 3).

Interactions of AgTx2 Mutants with KcsA-Kv1.6

As discussed above, residues of KcsA-Kv1.6 (Kv1.6) that interact with toxins form two clusters: the first one comprises the residues, which are specific for KcsA-Kv1.6 (Kv1.6), whereas the second cluster includes residues that are mainly invariant in relative Kv1-channels. It is reasonable to suppose that substitutions in toxin residues interacting with the first cluster can be used to modulate affinity and specificity of blockers to KcsA-Kv1.6 (Kv1.6). In addition, construction of such toxin mutants can help to verify the developed models in experiments and check reliability of molecular modeling predictions. We have produced four AgTx2 mutants having single point mutations (S7 K, S11G, K19S, R31G) and measured their binding to KcsA-Kv1.6. Mutant AgTx2(S7 K) was designed to verify a molecular modeling prediction that Ser7 is not involved in the interactions of AgTx2 with KcsA-Kv1.6 (or Kv1.6, Table 1). Similar *Kap* values obtained for AgTx2 (K_{ap} = 70 ± 10 pM) and AgTx2(S7 K) (K_{ap} = 55 ± 15 pM, Fig. 3c) supported this prediction. According to data presented in Table 1, substitution S11G should disrupt hydrogen bonds formed by Ser11 with channel residues and weaken toxin-channel interactions. Exactly, binding of KcsA-Kv1.6 to the toxin was considerably impaired by S11G mutation (K_{ap} = 350 ± 60 pM, Fig. 3c). To check the effect of ionic interaction of Lys19 with a channel (Table 1) and estimate its strength, this charged residue was replaced with serine. Competitive binding measurements revealed fivefold reduction of AgTx2(K19S) affinity to KcsA-Kv1.6 (K_{ap} = 370 ± 50 pM) as compared to AgTx2 (Fig. 3c), which was evidently associated with disappearance of the Lys19-related ionic bond with D55 of KcsA-Kv1.6. Involvement of another charged residue, Arg31, in ionic interactions with KcsA-Kv1.6 (Table 1) was confirmed by an increase in K_{ap} to 300 ± 80 pM after R31G substitution (Fig. 3c). Lys19 and Arg31 of AgTx2 interact with aspartates (D55 and D56) of KcsA-Kv1.6 (Table 1), which are a feature of Kv1.6 P-loops. Thus, disruption of these bonds accompanied with a decrease in stability of AgTx2-Kv1.6 complex could be a way to increase selectivity of toxin interactions with Kv1.3 and (or) Kv1.1.

Conclusion

As demonstrated, the developed cellular system, which is based on the membrane presentation of hybrid KcsA-Kv1.6 channel and fluorescent detection of pore blocker interactions, is a new convenient analytical tool for investigation of molecular determinants of affinity and specificity of peptide blockers to Kv1.6 pore. Fundamentally, this system utilizes evolution-related homology and structural similarity of pore domains of eukaryotic and bacterial potassium channels as well as accumulated knowledge on structural elements forming a toxin binding site in the outer vestibule of Kv1 channels. The presented results are a successful attempt to create artificial high-affinity membrane-embedded receptor and to control its expression, membrane transfer and presentation in *E.coli* cells by bioengineering means.

Comparative molecular modeling of toxin complexes with KcsA-Kv1.6 and Kv1.6 revealed reproduction of the binding mode and essential intermolecular bonds in both types of complexes that complementary validated an application of KcsA-Kv1.6-based system for investigation of toxin-Kv1.6 channel interactions. Moreover, KcsA-Kv1.6 system is suitable for seeking new peptide blockers in animal venoms, and these studies are in progress now.

Complexes of three recognized Kv1 channel blockers (AgTx2, OSK1 and KTx) with a pore domain of Kv1.6 channels, which were created for the first time using homology modeling approach, fill in the gap in our understanding of structural features of peptide blocker interactions with Kv1.6 channel. Ten channel residues participated in the toxin binding comprise two clusters: residues, which are situated in the P-

loop and vary in relative Kv1 channels and conserved residues, which are involved in interactions with toxins in different Kv1 channels. The first cluster can be a target to modulate (enhance or reduce) binding of designed peptide blockers to Kv1.6 as confirmed with point mutations introduced in AgTx2. Taking into account the published data, the second cluster seems to be a general basis for toxin binding to relative Kv1 channels.

Definitely, the rational design of selective peptide channel blockers, which are required in physiology investigations of Kv1 channels and in prospective medical applications, can be assisted with molecular modeling techniques. These computational experiments are intended to take into account fine features of multipoint peptide blocker interactions with several relative Kv1 channels.

Acknowledgments This work is supported by the Russian Science Foundation (grant no. 14-14-00239). LSM710 microscope was granted by the M.V. Lomonosov Moscow State University Program of Development.

Compliance with Ethical Standards

Conflict of Interests The authors declare that they have no conflict of interest.

References

Aiyar J, Withka JM, Rizzi JP, et al. (1995) Topology of the pore-region of a K+ channel revealed by the NMR-derived structures of scorpion toxins. Neuron 15:1169–1181

Aiyar J, Rizzi JP, Gutman GA, Chandy KG (1996) The signature sequence of voltage-gated potassium channels projects into the external vestibule. J Biol Chem 271:31013–31016. doi:10.1074/jbc.271.49.31013

Alessandri-Haber N, Alcaraz G, Deleuze C, et al. (2002) Molecular determinants of emerging excitability in rat embryonic motoneurons. J Physiol 541:25–39

Anh HN, Hoang VDM, Kudryashova KS, et al (2013) Hetlaxin, a new toxin from the Heterometrus laoticus scorpion venom, interacts with voltage-gated potassium channel Kv1.3. Dokl Biochem Biophys 449:109–111. doi:10.1134/S1607672913020142

Banerjee A, Lee A, Campbell E, MacKinnon R (2013) Structure of a pore-blocking toxin in complex with a eukaryotic voltage-dependent K+ channel. ElIfe 2:e00594. doi:10.7554/eLife.00594

Bergeron ZL, Bingham J-P (2012) Scorpion toxins specific for potassium (K+) channels: a historical overview of peptide bioengineering. Toxins (Basel) 4:1082–1119. doi:10.3390/toxins4111082

Brahmajothi MV, Morales MJ, Rasmusson RL, et al. (1997) Heterogeneity in K+ channel transcript expression detected in isolated ferret cardiac myocytes. Pacing Clin Electrophysiol 20:388–396

Chen PC, Kuyucak S (2009) Mechanism and energetics of charybdotoxin unbinding from a potassium channel from molecular dynamics simulations. Biophys J 96:2577–2588. doi:10.1016/j.bpj.2008.12.3952

Chen PC, Kuyucak S (2012) Developing a comparative docking protocol for the prediction of peptide selectivity profiles: investigation of potassium channel toxins. Toxins (Basel) 4:110–138. doi:10.3390/toxins4020110

Chung YH, Shin C, Kim MJ, et al. (2001) Immunohistochemical study on the distribution of six members of the Kv1 channel subunits in the rat cerebellum. Brain Res 895:173–177

Coetzee WA, Amarillo Y, Chiu J, et al. (1999) Molecular diversity of K+ channels. Ann N Y Acad Sci 868:233–285

Cui M, Shen J, Briggs JM, et al. (2002) Brownian dynamics simulations of the recognition of the scorpion toxin P05 with the small-conductance calcium-activated potassium channels. J Mol Biol 318:417–428. doi:10.1016/S0022-2836(02)00095-5

Davies AM, Batchelor TJP, Eardley I, Beech DJ (2002) Potassium channel KV alpha1 subunit expression and function in human detrusor muscle. J Urol 167:1881–1886

Dutertre S, Lewis RJ (2010) Use of venom peptides to probe ion channel structure and function. J Biol Chem 285:13315–13320. doi:10.1074/jbc.R109.076596

Eriksson MA, Roux B (2002) Modeling the structure of agitoxin in complex with the shaker K+ channel: a computational approach based on experimental distance. Biophys J 83:2595–2609. doi:10.1016/S0006-3495(02)75270-3

Gao Y, Garcia ML (2003) Interaction of agitoxin 2, charybdotoxin, and iberiotoxin with potassium channels: selectivity between voltage-gated and maxi-K channels. Proteins 52:146–154

Garcia ML, Garcia-Calvo M, Hidalgo P, et al. (1994) Purification and characterization of three inhibitors of voltage-dependent K+ channels from Leiurus Quinquestriatus Var. Hebraeus venom. Biochemistry 33:6834–6839

Gavrilovici C, Pollock E, Everest M, Poulter MO (2012) The loss of interneuron functional diversity in the piriform cortex after induction of experimental epilepsy. Neurobiol Dis 48:317–328. doi:10.1016/j.nbd.2012.07.002

Glazebrook PA, Ramirez AN, Schild JH, et al. (2002) Potassium channels Kv1.1, Kv1.2 and Kv1.6 influence excitability of rat visceral sensory neurons. J Physiol 541:467–482

Gonzalez C, Baez-Nieto D, Valencia I, et al. (2012) K+ channels: function-structural overview. Commun Phys 2:2087–2149. doi:10.1002/cphy.c110047

Gordon D, Chen R, Chung S-H (2013) Computational methods of studying the binding of toxins from venomous animals to biological ion channels: theory and applications. Physiol Rev 93:767–802. doi:10.1152/physrev.00035.2012

Gross A, Mackinnon R (1996) Agitoxin Footprinting the shaker Potassium Channel pore. Neuron 16:399–406

Hao J, Padilla F, Dandonneau M, et al. (2013) Kv1.1 channels act as mechanical brake in the senses of touch and pain. Neuron 77:899–914. doi:10.1016/j.neuron.2012.12.035

Hayes KC (2004) The use of 4-aminopyridine (fampridine) in demyelinating disorders. CNS Drug Rev 10:295–316

Hidalgo P, Mackinnon R (1995) Revealing the architecture of a K+ channel pore through mutant cycles with a peptide inhibitor. Science 268:307–310

Hoang AN, Vo HDM, Vo NP, et al. (2014) Vietnamese Heterometrus laoticus scorpion venom: evidence for analgesic and anti-inflammatory activity and isolation of new polypeptide toxin acting on Kv1.3 potassium channel. Toxicon 77:40–48. doi:10.1016/j.toxicon.2013.10.027

Jang SH, Ryu PD, Lee SY (2011) Dendrotoxin-κ suppresses tumor growth induced by human lung adenocarcinoma A549 cells in nude mice. J Vet Sci 12:35–40

Jorgensen WL, Maxwell DS, Tirado-rives J (1996) Development and testing of the OPLS all-atom force field on conformational energetics and properties of organic liquids. J Am Chem Soc 118:11225–11236

Jouirou B, Mosbah A, Visan V, et al. (2004) Cobatoxin 1 from Centruroides noxius scorpion venom: chemical synthesis, three-

dimensional structure in solution, pharmacology and docking on K+ channels. Biochem J 377:37–49. doi:10.1042/BJ20030977

Kirsch GE, Shieh CC, Drewe JA, et al. (1993) Segmental exchanges define 4-aminopyridine binding and the inner mouth of K+ pores. Neuron 11:503–512

Kohl B, Rothenberg I, Ali SA, et al. (2015) Solid phase synthesis, NMR structure determination of α-KTx3.8, its in silico docking to Kv1.X potassium channels, and electrophysiological analysis provide insights into toxin-channel selectivity. Toxicon 101:70–78. doi:10.1016/j.toxicon.2015.04.018

Kudryashova KS, Nekrasova OV, Kuzmenkov AI, et al. (2013) Fluorescent system based on bacterial expression of hybrid KcsA channels designed for Kv1.3 ligand screening and study. Anal Bioanal Chem 405:2379–2389. doi:10.1007/s00216-012-6655-6

Kuzmenkov AI, Vassilevski AA, Kudryashova KS, et al. (2015) Variability of Potassium Channel blockers in Mesobuthus eupeus scorpion venom with focus on Kv1.1: AN INTEGRATED TRANSCRIPTOMIC AND PROTEOMIC STUDY. J Biol Chem 290:12195–121209. doi:10.1074/jbc.M115.637611

Legros C, Pollmann V, Knaus HG, et al. (2000) Generating a high affinity scorpion toxin receptor in KcsA-Kv1.3 chimeric potassium channels. J Biol Chem 275:16918–16924. doi:10.1074/jbc.275.22.16918

Legros C, Schulze C, Garcia ML, et al. (2002) Engineering-specific pharmacological binding sites for peptidyl inhibitors of potassium channels into KcsA. Biochemistry 41:15369–15375

Ling J, Yingliang W (2007) Molecular mechanism of the sea anemone toxin ShK recognizing the Kv1.3 channel explored by docking and molecular dynamic simulations. J Chem Inf Model 47:1967–1972. doi:10.1021/ci700178w

Lipkind GM, Fozzard HA (1997) A model of scorpion toxin binding to voltage-gated K+ channels. J Membr Biol 158:187–196. doi:10.1007/s002329900256

MacKinnon R, Cohen S, Kuo A, et al. (1998) Structural conservation in prokaryotic and eukaryotic potassium channels. Science 280:106–109

Matus-Leibovitch N, Vogel Z, Ezra-Macabee V, et al. (1996) Chronic morphine administration enhances the expression of Kv1.5 and Kv1.6 voltage-gated K+ channels in rat spinal cord. Brain Res Mol Brain Res 40:261–270

Mondal S, Babu RM, Bhavna R, Ramakumar S (2007) In silico detection of binding mode of J-superfamily conotoxin pl14a with Kv1.6 channel. In Silico Biol 7:175–186

Mouhat S, Visan V, Ananthakrishnan S, et al. (2005) K+ channel types targeted by synthetic OSK1, a toxin from Orthochirus scrobiculosus scorpion venom. Biochem J 385:95–104. doi:10.1042/BJ20041379

Mouhat S, Teodorescu G, Homerick D, et al. (2006) Pharmacological profiling of Orthochirus scrobiculosus toxin 1 analogs with a trimmed N-terminal domain. Mol Pharmacol 69:354–362. doi:10.1124/mol.105.017210

Naranjo D, Miller C (1996) A strongly interacting pair of residues on the contact surface of charybdotoxin and a shaker K+ channel. Neuron 16:123–130. doi:10.1016/S0896-6273(00)80029-X

Nekrasova OV, Ignatova AA, Nazarova AI, et al. (2009a) Recombinant Kv channels at the membrane of *Escherichia coli* bind specifically agitoxin2. J NeuroImmune Pharmacol 4:83–91. doi:10.1007/s11481-008-9116-4

Nekrasova O, Tagway A, Ignatova A, et al. (2009b) Studying of membrane localization of recombinant potassium channels in E.Coli. Acta Nat 1:91–95

Novoseletsky VN, Volyntseva AD, Shaitan KV, et al. (2016) Modeling of the binding of peptide blockers to voltage-gated potassium channels: approaches and evidence. Acta Nat 8:35–46

Park WS, Firth AL, Han J, Ko EA (2010) Patho-, physiological roles of voltage-dependent K+ channels in pulmonary arterial smooth muscle cells. J Smooth Muscle Res 46:89–105

Pérez-Verdaguer M, Capera J, Serrano-Novillo C, et al. (2016) The voltage-gated potassium channel Kv1.3 is a promising multitherapeutic target against human pathologies. Expert Opin Ther Targets 20:577–591. doi:10.1517/14728222.2016.1112792

Pyrkov T, Chugunov A, Krylov N, et al. (2009) PLATINUM: a web tool for analysis of hydrophobic/hydrophilic organization of biomolecular complexes. Bioinformatics 25:1201–1202

Ranganathan R, Lewis JH, Mackinnon R (1996) Spatial localization of the K+ channel selectivity filter by mutant cycle – based structure analysis. Neuron 16:131–139

Rashid MH, Kuyucak S (2012) Affinity and selectivity of ShK toxin for the Kv1 potassium channels from free energy simulations. J Phys Chem B 116:4812–4822. doi:10.1021/jp300639x

Rashid MH, Kuyucak S (2014) Free energy simulations of binding of HsTx1 toxin to Kv1 potassium channels: the basis of Kv1.3/Kv1.1 selectivity. J Phys Chem B 118:707–716. doi:10.1021/jp410950h

Sali A, Blundell T (1993) Comparative protein modelling by satisfaction of spatial restraints. J Mol Biol 234:779–815

Schmidt K, Eulitz D, Veh RW, et al. (1999) Heterogeneous expression of voltage-gated potassium channels of the shaker family (Kv1) in oligodendrocyte progenitors. Brain Res 843:145–160

Shah NH, Aizenman E (2014) Voltage-gated potassium channels at the crossroads of neuronal function, ischemic tolerance, and neurodegeneration. Transl Stroke Res 5:38–58. doi:10.1007/s12975-013-0297-7

Tian C, Zhu R, Zhu L, et al. (2014) Potassium channels: structures, diseases, and modulators. Chem Biol Drug Des 83:1–26. doi:10.1111/cbdd.12237

Wang X, Umetsu Y, Gao B, et al. (2015) Mesomartoxin , a new K v 1. 2-selective scorpion toxin interacting with the channel selectivity filter. Biochem Pharmacol 93:232–239. doi:10.1016/j.bcp.2014.12.002

Webb B, Sali A (2016) Comparative protein structure modeling using MODELLER. Curr Protoc Bioinformatics 54. doi:10.1002/cpbi.3

Wu Y, Cao Z, Yi H, et al. (2004) Simulation of the interaction between ScyTx and small conductance calcium-activated potassium channel by docking and MM-PBSA. Biophys J 87:105–112. doi:10.1529/biophysj.103.039156

Xiang Z (2006) Advances in homology protein structure modeling. Curr Protein Pept Sci 7:217–227

Yu K, Fu W, Liu H, et al. (2004) Computational simulations of interactions of scorpion toxins with the voltage-gated potassium Ion Channel. Biophys J 86:3542–3555. doi:10.1529/biophysj.103.039461

Yu L, Sun C, Song D, et al. (2005) Nuclear magnetic resonance structural studies of a potassium channel-charybdotoxin complex. Biochemistry 44:15834–15841. doi:10.1021/bi051656d